Noncontact measurement of sub-micrometer ultrasonic vibration by near-field microwave

View Online   Export Citation   CrossMark

Cuiling Peng, Xiaolong Chen,[a]) Huiting Huan,[a]) Liping Huang, Jinsong Zhan, and Lixian Liu

AFFILIATIONS

Xi'an Key Laboratory of Intelligent Instrument and Packaging Test, School of Mechano-Electronic Engineering, Xidian University, Xi'an 710071, China

Note: This paper is part of the Special Topic on Non-Invasive and Non-Destructive Methods and Applications Part II.
[a])**Authors to whom correspondence should be addressed:** xlchen@mail.xidian.edu.cn and hthuan@xidian.edu.cn

ABSTRACT

In this article, we proposed a noncontact testing scheme for micrometer to sub-micrometer level ultrasonic vibration mainly generated by laser ultrasound upon the novel utilization of near-field microwaves. The measurement was performed based on a Ku-band near-field resonator-probe, which was optimized to perceive the low amplitude out-of-plane vibration in the ultrasonic range. A near-field electromagnetic measurement theory was established to help analyze the sensitivity and responsivity of the resonator-probe outfit. The electric field parameters were extracted with respect to the port based on a lumped-circuit model, which was further validated using a finite-element model. Experiments were carried out with respect to a piezoelectric ceramic disk designed to generate vibrations of desired amplitude, which is compatible to that in laser ultrasonic testing. The accuracy of the technique was assessed by comparing with the laser vibrometer measurement results. It was verified that the proposed near-field microwave probe can achieve considerable accuracy in perceiving sub-micrometer ultrasonic vibration up to 180 kHz.

I. INTRODUCTION

Laser ultrasonics is a noncontact and nondestructive testing (NDT) technique that has been developed in a number of applications in industrial and medical scenarios such as evaluating metal residual stress,[1] detecting defects in composites,[2] testing biological tissues,[3] etc. From a physical viewpoint, the incident laser excites stress/strain waves above 20 kHz in the tested specimen through the effect of thermoelectricity or laser ablation[4] and generates ultrasonic signals of various modes and waveforms.[5] The thermoelastic effect plays a more important role in NDT because of its absolutely nondestructive feature in producing thermal expansion with respect to the sample at a low incident laser density (lower than 10^7 W/cm^2).[6] To obtain defective information in materials, pulsed and harmonic modulated lasers are generally adopted in practice. The amplitude of a laser-generated ultrasonic signal highly depends on the laser energy/power with regard to the time- and frequency-domain laser ultrasound principles.[7–9] In recent years, the use of continuous-wave (CW) diode lasers has been verified by researchers in producing harmonic thermoelastic waves, which were used to detect elastic properties and defects inside the sample[9] and thereby

facilitate flexible and cost-effective NDT modality. However, a CW laser generates ultrasonic vibration of lower amplitude in the sub-micrometer level,[10] which is very difficult to detect. The ultrasonic detectability further deteriorates with increasing frequency, which limits the application of frequency-domain laser ultrasonics in the testing surface and buried defects within elastic solids.[11]

In most cases, ultrasonic vibration at the sub-micrometer level was tested with contact sensors such as accelerometers,[12] piezoelectric devices,[13] and strain gauges.[14] The performance of contacting vibration measurement depends upon the coupling conditions (e.g., the impedance matching conditions) between the chosen transducers and samples.[15] For noncontact approaches, the optical method amplifies laser ultrasonic surface displacement by means of either an optical lever or interferometry.[16,17] Advantages of the optical method are its ultra-wide bandwidth and good sensitivity, which make it practically useful in scenarios such as machinery,[18] medication,[19] and civil engineering.[20] However, the excellent performance of the laser ultrasonic vibration measurement lies in its sophisticated setup and good surface finish of the measured

objects.[21] It is still necessary to develop other useful modalities to overcome these disadvantages in vibrometry.

Near-field microwave probing is currently being observed as a powerful tool for testing electromagnetic properties of electronic integrated circuits.[22,23] Its usefulness has been proven by many researchers. Gao and Xiang established a near-field method to achieve highly sensitive perception of local change of dielectric properties and intermediate probing distance.[24] The vibrational signal was characterized in terms of back-propagated microwaves in the far-field. In the near-field range, microwave probes converge the electromagnetic field in the vicinity of the probe tip,[25–27] which makes the evanescent field extremely sensitive to displacement. By specifically designing the near-field probe with a suitable tip, it is expected that highly sensitive measurement of ultrasonic vibrations within the sub-micrometer range is achievable. Additionally, the near-field microwave method focuses on a much smaller localized spatial area and does not involve the detection of reflected waves. It has advantages in cost-effective instrumentation in specific applications.

This work aims to develop a framework of sensing the harmonic vibration at the sub-micrometer level based on near-field microwave testing. A compatible near-field ultrasonic vibration probe was devised and validated with the finite-element method (FEM). Both theoretical and experimental results were obtained to show the possibility and appropriateness of the method.

II. METHOD AND MATERIAL

A. The sample under test

Early reports have shown that the amplitude of laser induced ultrasound is at the level of sub-micrometer range when staying within the thermoelastic regime.[28] In order to materialize controllable ultrasonic vibration of the same level, a copper–lead zirconate titanate composite piezoelectric disk (consists of a copper disk with a radius of 13.5 mm and a lead zirconate titanate disk with a radius of 9.25 mm) with surface roughness of $6 \mu m$[29] was used as the sample. A piezoelectricity–elasticity coupling finite-element analysis using COMSOL® Multiphysics was carried out to examine the vibrational feature of the sample. As shown in Fig. 1, the disk was subjected to triangular circumferential fixation. The eigenfrequencies of the transducer stay within audible range, which ensures a much lower vibration amplitude in the designated ultrasonic frequency range, resulting in a voltage-controlled sub-micrometer level ultrasonic vibration. The maximum vibration amplitude varies with frequency and changes with voltage linearly.

The experimental setup is shown in Fig. 2. The experimental system consists of an RF signal source (Ceyear®, AV1463, 250 kHz–40 GHz), laser vibrometer (Polytec®, VibroFlex-series), lock-in amplifier (Zurich Instruments®, MFLI, 5 MHz), coaxial resonant cavity (CRC) probe, and other microwave devices. The piezoelectric composite transducer under test was placed close to the microwave
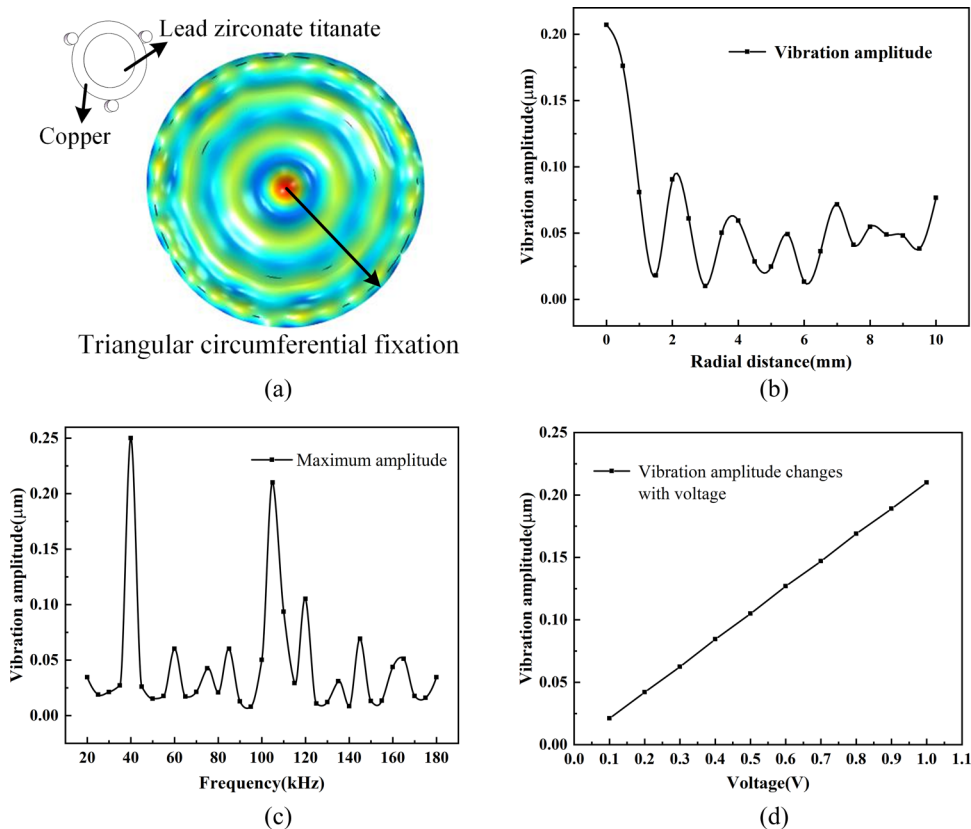
FIG. 1. The FEM simulation of (a) the piezoelectric disk operating at 80 kHz and the color-map indication of vibration amplitude, (b) the vibration amplitude along the arrow-line in (a), (c) the maximum vibration amplitude changes with frequency, and (d) the maximum vibration amplitude changes with voltage at 80 kHz.

near-field probe, which will be elaborated in Appendix. Micrometer stages were used to delicately control the probe-sample distance and the in-plane scanning movement. An RF source (18.23 GHz, 5 dBm) generated signal equivalent to the resonant frequency of the CRC probe, and electrical driving signals were fed to the composite piezoelectric disk. The coupler separated the signal into two channels with equal power, which were used as the carrier and reference, respectively. The circulator transmitted the carrier signal to the probe and received a vibration modulated signal. The ultrasonic signal was demodulated in a lock-in amplifier after mixed with the reference and low-pass (1 MHz bandwidth) filtered. To validate the correctness of the FEM simulation on the piezoelectric disk, the sample was tested with a high-sensitive laser vibrometer to provide reference amplitude.

B. Design of the vibrational sensor

Conventional microwave field is limited by the Abbe diffraction limit of half wavelength ($\lambda/2$).[30] It is almost impossible to deconvolute the sub-micrometer displacement from the detected microwave signal. In the near-field range, nevertheless, the microwave field is confined to a limited space around the probe tip, which has considerable resolution and sensitivity in near-field measurement. In this work, the near-field probe is a CRC designed and outfitted with a needle-like probe. The CRC probe converges most of the electromagnetic energy inside the cavity, being less affected by the external RF

electromagnetic background. As shown in Fig. 3, the CRC probe consists of a monopole, a sharpened tungsten needle (the probe), and a cylindrical coaxial resonant cavity. A small hole in the center of the cavity bottom allows the probe tip to extend out and confines the electromagnetic field around the tip. A monopole was used as an input–output-dual-utility port. The usefulness of the CRC probe has also been validated by several applications in dielectric measurement,[31,32] yet it has not been used to sensing the dynamic motion of high frequency and small amplitude. To design a surface fluctuation sensitive CRC probe properly, we should consider two factors in terms of the carrier microwave band and the S-parameters on the port. The near-field CRC probe was designed in the K-band (~18 GHz), far higher than the operation frequencies in previous reports.[31] On the other hand, the dimensions of the probe tip should be optimized to reach a high sensitivity in perceiving the out-of-plane displacement. Detailed information is provided in the Appendix.

C. Dynamic theory of microwave near-field

The interpretation of the near-field microwave around the probe tip has been systematically established using a quasi-static method by Gao and Xiang.[24] However, this theory needs to be modified to suit the measurement and explain the dynamic signal variation. Considering the fact that the ultrasonic frequency is much lower than the microwave, it is reasonable to treat the out-of-plane
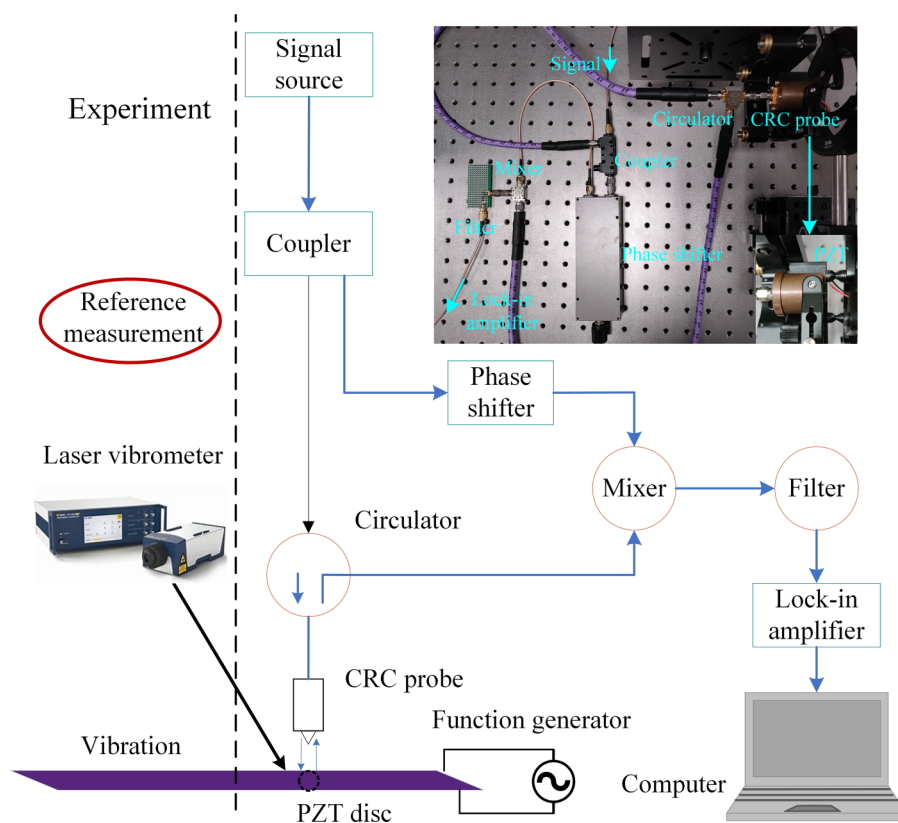
FIG. 2. Block diagram of the near-field microwave measurement system.
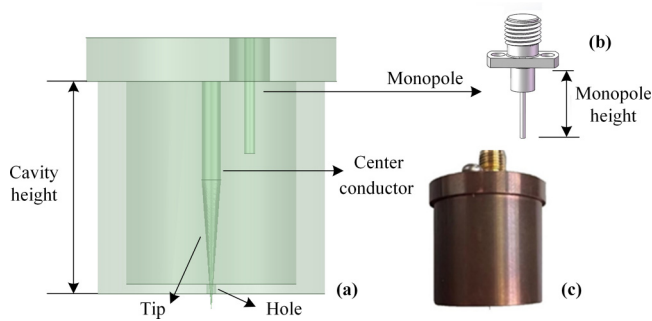
FIG. 3. Schematic of the CRC probe with a coupling monopole (b) at the top of the cavity. (c) Photo of the CRC probe.

FIG. 4. The equivalent lumped model of the tip–sample interaction.

vibration as slow and uniform motion. The interaction between the sample and probe can be explained using an equivalent lumped model shown in Fig. 4.[25,33] When the sample–tip distance changes slightly, the near-field evanescent field is reshaped as a result of varied boundary conditions, and the coupling capacitance C_1 changes accordingly, resulting in the shift of resonant frequency. Such changes can be modeled using the perturbation theory considering the dielectric constant with respect to the sample as[34]
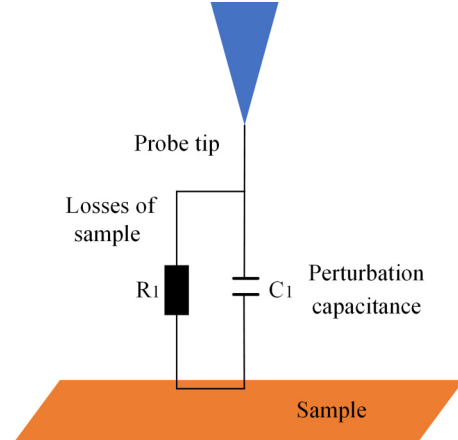
$$\frac{\Delta f}{f} = \frac{f - f'}{f} = \frac{\iiint_{V_1} (\mathbf{E} \cdot \mathbf{D}_0 - \mathbf{E}_0 \cdot \mathbf{D}) - (\mathbf{H} \cdot \mathbf{B}_0 - \mathbf{H}_0 \cdot \mathbf{B}) dv}{\iiint_V (\mathbf{E}_0 \cdot \mathbf{D} - \mathbf{H}_0 \cdot \mathbf{B}) dv}$$

$$= \frac{\iiint_{V_1} [(\varepsilon_0 - \varepsilon_r)\mathbf{E}_0 \cdot \mathbf{E} - (\mu_0 - \mu_r)\mathbf{H}_0 \cdot \mathbf{H}] dv}{\iiint_V (\mathbf{E}_0 \cdot \mathbf{D} - \mathbf{H}_0 \cdot \mathbf{B}) dv}, \quad (1)$$

where $\mathbf{E}_0$ and $\mathbf{H}_0$ are the electric and magnetic fields with respect to the reference (static) state, respectively, $\mathbf{E}_1$ and $\mathbf{H}_1$ are the corresponding fields under vibrational state, V and V_1 refer to the cavity volume and the volume of the perturbing object, respectively, f and f' are the resonant frequencies without and with the existence of vibrational perturbation, respectively, ε_0 and μ_0 are the permittivities of free space, ε_r and μ_r are the relative permittivities of the sample, and $\nabla \times \mathbf{E}_i = -j2\pi f_i \mathbf{B}_i$ and $\nabla \times \mathbf{H}_i = -j2\pi f_i \mathbf{D}_i$ are Maxwell's curl equations used to calculate $\mathbf{D}$ and $\mathbf{B}$, respectively.

The system was configured as a noncontact measurement one. Therefore, an air gap exists between the tip and the sample, which is much smaller than the microwave wavelength. In this case, the tip is treated as a perfectly conductive sphere and the corresponding electric field $\mathbf{E}_1$ can be analyzed by the quasi-static theory.[24,35] Using the method of images,[36,37] the electric field can be represented by a series of image charges q_n redistribution on the tip when the tip scans directly on the sample surface, i.e.,

$$q_n = \frac{1}{n}\left(\frac{\varepsilon - \varepsilon_0}{\varepsilon + \varepsilon_0}\right)^{n-1} q, \quad (2a)$$

$$q = 4\pi\varepsilon_0 R U_0, \quad (2b)$$

where R is the tip radius and U_0 is the tip voltage of the microwave cavity. The image charges and the air gap length are physically connected in terms of an iterative form as

$$q_n = \frac{1}{1 + a' + a_{n-1}}\left(\frac{\varepsilon - \varepsilon_0}{\varepsilon + \varepsilon_0}\right)^{n-1} q = t_n q, \quad (3a)$$

$$t_n = \frac{b t_{n-1}}{1 + a' + a_{n-1}} = \frac{1}{n} b^{n-1}, \quad (3b)$$

$$a_n = a_1 + \frac{1}{a_1 + a_{n-1}} = 1 + a' - \frac{1}{1 + a' + a_{n-1}}, \quad (3c)$$

where $b = (\varepsilon - \varepsilon_0)/(\varepsilon + \varepsilon_0)$ and $a' = g/R$. The initial values for a_n and t_n are $a_1 = 1 + g/R$ and $t_1 = 1$. The electrostatic field is formed as

$$\mathbf{E}_1 = \sum_{n=1}^{\infty} \frac{q_n}{2\pi\varepsilon_0} \frac{(\mathbf{r} - \mathbf{r}_n)}{|\mathbf{r} - \mathbf{r}_n|^3}$$

$$= \frac{4\pi\varepsilon_0 R U_0}{2\pi(\varepsilon + \varepsilon_0)} \sum_{n=1}^{\infty} \frac{b t_n}{1 + g/R + a_n} \frac{x\mathbf{e}_x + y\mathbf{e}_y + (z + g)\mathbf{e}_z}{[x^2 + y^2 + (z + g)^2]^{\frac{3}{2}}}, \quad (4)$$

where $\mathbf{e}_x$, $\mathbf{e}_y$, and $\mathbf{e}_z$ are unit vectors along the x, y, and z axis, respectively. As the tip and sample stay in-line along the z axis, the perturbed electric field as a function of z and air gap length g can be simplified to

$$E_1[g(t)] = \frac{2\varepsilon_0 R U_0}{(\varepsilon + \varepsilon_0)g(t)^2} \sum_{n=1}^{\infty} \frac{b t_n}{1 + g(t)/R + a_n}$$

$$= \frac{2\varepsilon_0 R U_0}{(\varepsilon + \varepsilon_0)g(t)^2}\left[-\frac{\ln(1 - b)}{b} - 1\right], \quad (5)$$

by substituting Eqs. (2) and (3) into Eq. (4). Equation (5) indicates
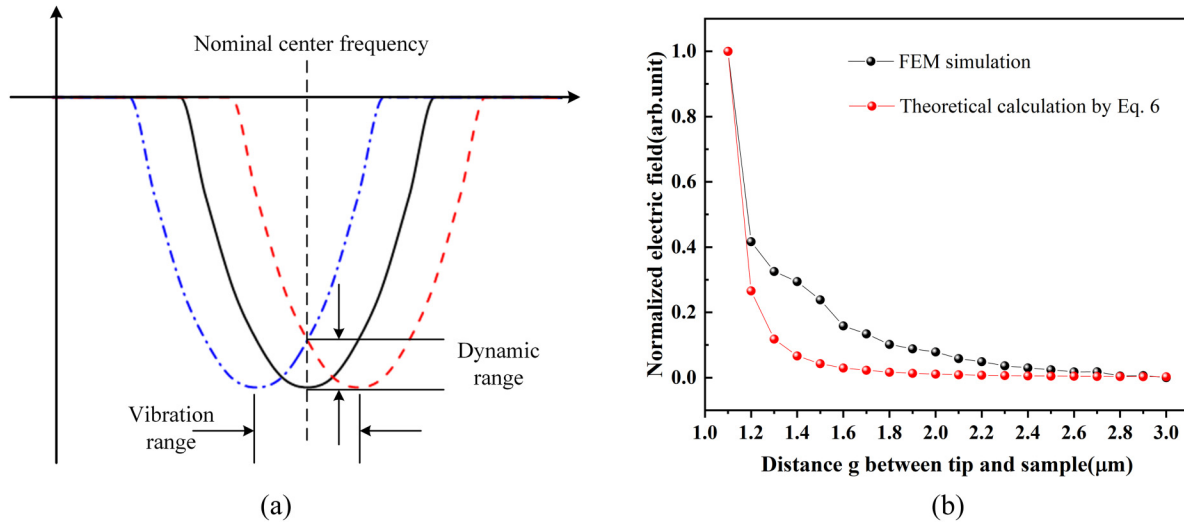
FIG. 5. The change of electric field as a function of tip–sample distance: (a) an interpretation of the resonant frequency shifting with the sample–tip distance; (b) the change of electric field at nominal center frequency *f* as a function of stationary *g*.

the amplitude of electric field is inversely proportional to the square of the tip–sample distance g. In the case of harmonic modulation, the ultrasonic vibration is described in terms of a periodic cosine function, i.e., $g(t) = g_0 + g_\varepsilon \cos(\omega t + \varphi)$, with g_ε denoting the small vibrational amplitude; substituting it into Eq. (5), we have the varied electric field. Applying Taylor's expansion with respect to g_ε and reserve to the linear term, we have

$$
\begin{aligned}
U(t) = E_1[g(t)]g(t) &= -\frac{2\varepsilon_0 R U_0 [b^{-1} \ln(1-b) + 1]}{(\varepsilon + \varepsilon_0)g(t)} \\
&\approx -\frac{2\varepsilon_0 R U_0 [b^{-1} \ln(1-b) + 1]}{(\varepsilon + \varepsilon_0)g_0} \\
&\quad \times [1 - g_0^{-1} g_\varepsilon \cos(\omega t + \varphi)].
\end{aligned}
\tag{6}
$$

Equation (6) suggests that the signal is proportional to the harmonic displacement around g_0, where g_ε is much smaller than g_0. The feasibility of the proportional relationship between the electric field and the signal will be further verified.

III. RESULTS AND DISCUSSION

A. Numerical validation of measurement theory

The sample was set $1\,\mu$m away from the tip, ensuring a near-field range. The electric amplitude at the lumped port was then calculated and shown in Fig. 5. As expected, the electric amplitude decays almost exponentially with increasing tip–sample distance g. The results calculated by Eq. (6) and the FEM exhibit a similar trend. However, due to the truncation in the series during the theoretical calculation, there exists discrepancy for electric amplitude between 1.2 and $2.4\,\mu$m range of g. Both analytical and numerical results indicate a steep slope of electric field change for tip–sample

distance $g < 2\,\mu$m. In this regime, a slight vibration in sample surface can give rise to a large change in the electric field, which makes the testing modality possible in measuring the sub-micrometer ultrasonic surface movement.
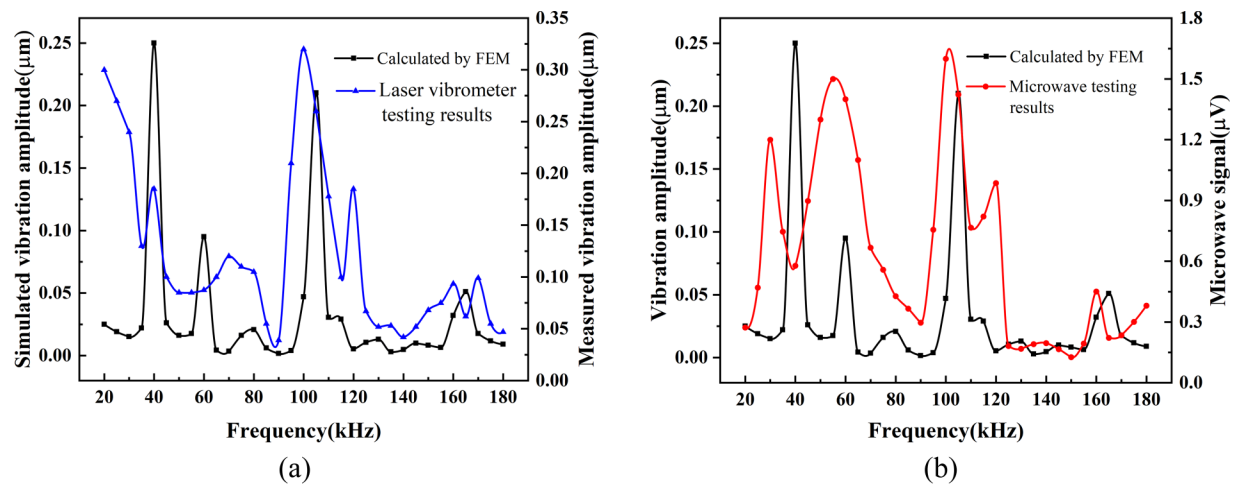
B. Experimental validation

The transmission performance of the CRC probe described in the Appendix was first analyzed in terms of S_{11} shown in Fig. 6. Due to the random machining errors and surface losses, the measured resonant frequency 18.23 GHz was slightly displaced from
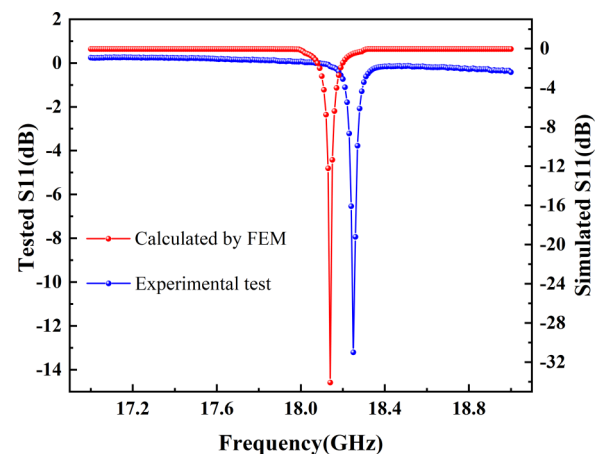
**FIG. 6.** S_{11} comparison between simulation and product.

FIG. 7. Comparison between (a) FEM simulation and the results obtained by a commercial laser vibrometer; (b) FEM simulation and the results from microwave near-field measurement.

the simulation frequency 18 GHz. There exists discrepancy in the S_{11} measurement results compared with the simulation results.

A single frequency microwave of 18.23 GHz is employed to perform the experiment. The amplitude from FEM simulation and laser vibrometer are compared in Fig. 7(a), and the near-field microwave measurement results compared with FEM simulation are showed in Fig. 7(b). Both tests were conducted under the same condition (driving AC voltage, sample fixation, targeting area in the sample surface, etc.). The results show the order of the sub-micrometric vibration level, in quantitative agreement with the foregoing simulation.

The minimum vibration value measured by the laser vibrometer is about 0.05 μm. The comparison results show the near-field microwave method measured vibration at a similar level to the laser vibrometer. As the spot size of the focused laser is different from the probe tip area, discrepancy appears in the measurement results between the two methods. It can be observed that the testing results from CRC outfit show considerable analogy with the results obtained from the optical vibrometer and FEM for frequency above 50 kHz, with the maxima coincide with respect to the same frequency (~100 kHz), and the microwave measurement results show more resemblance to the simulation results than the laser vibration
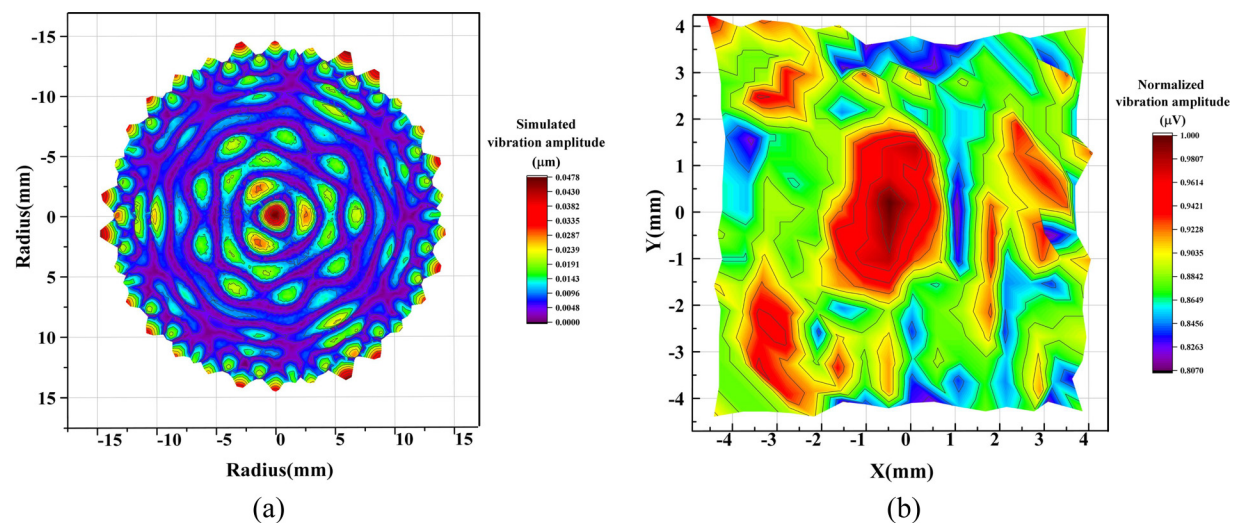
FIG. 8. The vibration amplitude (a) simulation results of the piezoelectric disk in 100 kHz; (b) recorded scan results by microwave probe.

measurement due to the higher resolution CRC probe mentioned in the Appendix. The discrepancy that occurs below 40 kHz can be resorted to the existence of $1/f$ noise in the experimental components, which vanishes with increasing frequency. There still exists some inconsistency as the probe and the sample cannot be kept ideally in-line and perpendicular. The experiments verified the feasibility of near-field single point sub-micrometer vibration probing by near-field microwave. The measurement resolution with a probe tip radius in the micrometer range is higher than the laser vibrometer with spot size in the order of millimeter or sub-millimeter. For very rough surfaces, the microwave near-field probe measurement method is more suitable than the laser method. The following scanning experiments can further verify the advantages of the near-field microwave method.

A probe scanning test was further conducted as an additional validation with respect to 100 kHz ultrasonic vibration. The scan area is $8 \times 8 \, \text{mm}^2$ in the center area with 0.2 mm increment, as shown in Fig. 8(a). The absolute value of the vibration amplitude decreases from the center to the circumference. The deconvoluted image (the vibrometric graph) shows excellent agreement with the simulated result in mapping the correct location of the central peak and the three neighboring lower peaks that are generated as a result of three-point-circumferential fixation. The microwave test is carried out in a small area near the tip, which cannot reach the same resolution as the simulation. In further quantitative measurements, the probe needs to be improved for a more accurate scan result.

Further improvement should be considered to overcome the limitations presented in the near-field testing system. It is necessary to further study the noise composition in the system, and the electromagnetic compatibility design should be optimized. The structure of the resonator can be further improved to achieve a higher quality factor.

IV. CONCLUSION

In this work, we have developed a sub-micrometer vibration measurement system based on near-field microwaves. A near-field CRC probe was designed and fabricated to perceive subtle out-of-plane displacement using electromagnetic evanescent waves. The physical basis for the noncontact measurement was established and verified by a series of FEM simulations. The experiments revealed that the near-field microwave measurement results agree well with the reference data from both the commercial vibrometer and the FEM. The excellent performance of the microwave near-field vibration measurement was further verified with a scan test.

ACKNOWLEDGMENTS

AUTHOR DECLARATIONS
Conflict of Interest

The authors have no conflicts to disclose.

DATA AVAILABILITY

The data that support the findings of this study are available within the article.

APPENDIX: DESIGN AND OPTIMIZATION OF THE SENSOR

The resonance frequency of the CRC probe is mainly determined by the length and radius of the cavity. The former was directly linked with the resonant wavelength λ by the following equation:[37]

$$l = \frac{2p - 1}{4}\lambda. \tag{A1}$$

The constant p is an integer that denotes the electromagnetic mode inside the CRC. In order to ensure the resonator can work at the TEM propagation mode, the radial dimensions of the CRC need to satisfy the basic working conditions of the coaxial cable,

$$\frac{\pi}{2}(D + d) < \lambda, \tag{A2}$$

where D and d are the outer and inner diameters, respectively.

Figure 9 shows the amplitude of the electric field around the tungsten tip at the resonance frequency in the absence of the sample. Fields in the vicinity of the probe tip exhibit near-field features. As the energy radiation range is limited to the probe tip, samples can be divided into tiny modules for measurement. According to the FEM simulation results, the measurement resolution of the CRC probe is approximately three times the size of the tip radius. As the surface roughness of the sample is an invariant in the vibration measurement, we can get the correct vibration measurement result as long as we can keep the distance between the sample and the needle tip a constant.
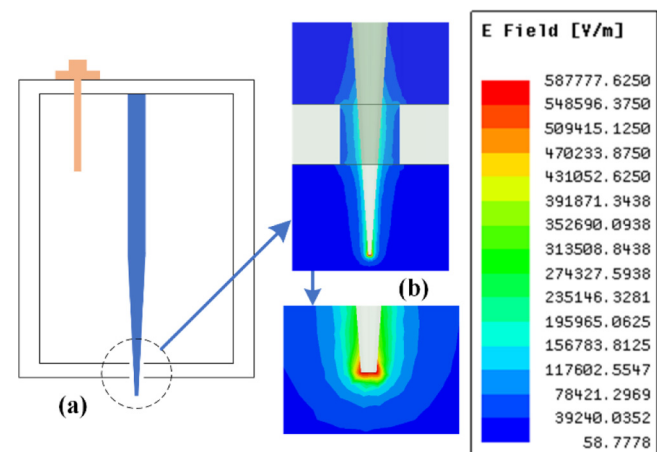
FIG. 9. The amplitude of the simulated electric fields at resonance frequency within the near-field range: (a) the schematic diagram of CRC probe; (b) the simulated electric fields around the tip.
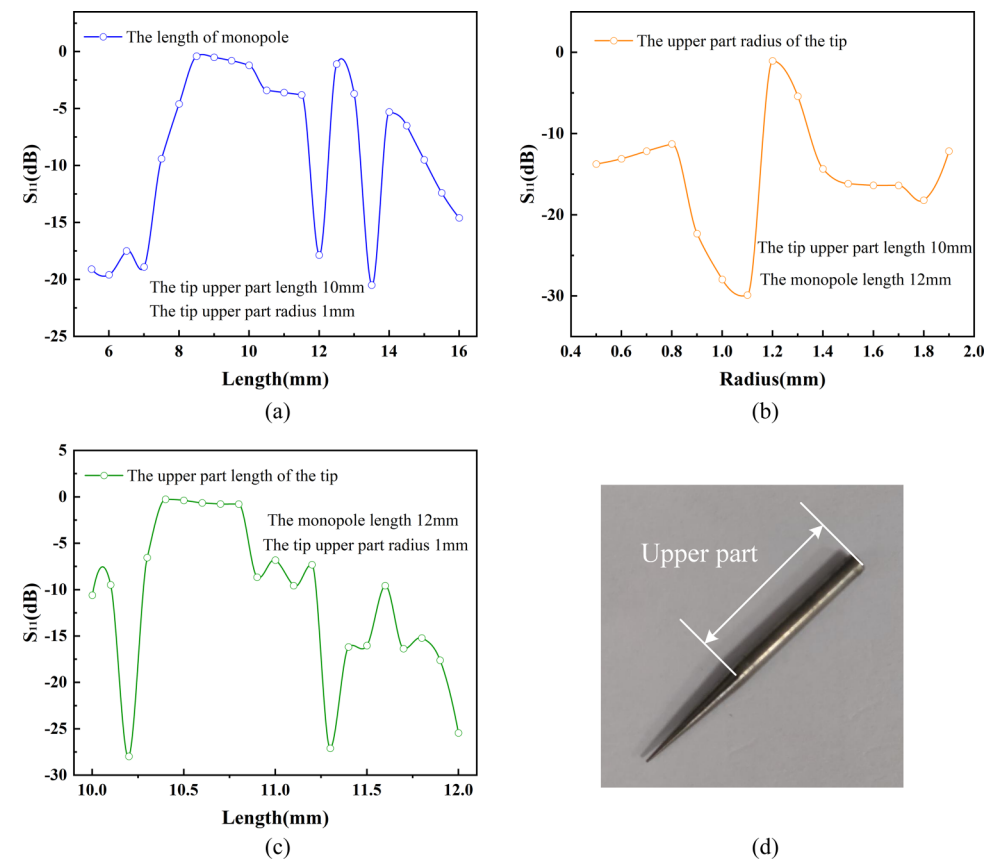
FIG. 10. Energy coupling as a function of dimensional parameters of the monopole and the center conductor: (a) L_m simulation with $R_t = 1$ and $L_t = 10$ mm; (b) R_t simulation with $L_m = 12$ and $L_t = 10.2$ mm; (c) L_t simulation with $L_m = 12$ and $R_t = 1$ mm.

The goal of optimizing the CRC probe is to ensure best performance in perceiving out-of-plane displacement. A higher Q factor is good in resonators at a single frequency. A higher Q factor results in a higher peak, which means more energy transmission and reception. So, the smaller and steeper the S_{11} parameter, the higher the energy coupling efficiency of the CRC outfit. This work was done with the help of an integrated FEM software (ANSYS® HFSS), and the results can be obtained by setting various dimensional parameters for the CRC probe. The choice of resonant frequency is directly related to the structure of the CRC and the coaxial tungsten probe as well.

The simulated results are shown in Fig. 10; the establishment of the model is carried out in the air box to simulate the distribution of the electric field in the actual test. The monopole length L_m, the tip upper part radius R_t, and length L_t were set as the independent variables in the optimization, in order to get better energy transmission S_{11}. The coaxial resonant cavity is designed by using Eqs. (A1) and (A2), verifying with an additional FEM calculation, as shown in Table I. To obtain a better energy coupling efficiency, lengths of the monopole and upper part of the tip are set as 12 and 10.2 mm, respectively, and the upper part radius of the center conductor is 1.1 mm (within the optimal range). The resolution will increase as the tip radius decreases, and the tip radius is designed as 0.025 mm considering the machine shop machining precision. The dimensions of the CRC probe were designed to be 26.5 mm in length and 11.8 mm in radius.

TABLE I. The design parameters for the CRC outfit.

Parameters	Material	Dimension (mm)
Cavity height	Copper	26.5
Cavity radius	Copper	11.8
Center conductor radius	Copper	1.1
Tip height	Tungsten	13.3
Tip lower radius	Tungsten	0.025
R_t	Tungsten	1
L_t	Copper	10.2
L_m	Copper	12

REFERENCES

[1]Y. Zhan, C. Liu, J. Zhang, G. Mo, and C. Liu, "Measurement of residual stress in laser additive manufacturing TC4 titanium alloy with the laser ultrasonic technique," Mater. Sci. Eng. A **762**, 138093 (2019).

[2]L. Liu, C. Guo, L. Wang, and H. Mei, "Nondestructive visualization and quantitative characterization of defects in silicone polymer insulators based on laser shearography," IEEE Sens. J. **19**(15), 6508–6516 (2019).

[3]J. N. Bixler, B. H. Hokr, M. L. Denton, G. D. Noojin, A. D. Shingledecker, H. T. Beier, R. J. Thomas, B. A. Rockwell, and V. V. Yakovelv, "Assessment of tissue heating under tunable near-infrared radiation," J. Biomed. Opt. **19**(7), 70501 (2014).

[4]*Laser Ultrasonic Thermoelastic/Ablation Generation with Laser Interferometric Detection in Graphite/Polymer Composites*, edited by J. N. Caron, J. B. Mehl, and K. V. Steiner (Springer US, 1996).

[5]D. A. Hutchins, F. Nadeau, and P. Cielo, "A pulsed photoacoustic investigation of ultrasonic mode conversion," Can. J. Phys. **64**(9), 1334–1340 (1986).

[6]S. J. Davies, C. Edwards, G. S. Taylor, and S. B. Palmer, "Laser-generated ultrasound: Its properties, mechanisms and multifarious applications," J. Phys. D: Appl. Phys. **26**(3), 329 (1999).

[7]O. Emile and J. Emile, "Laser-induced vibration of a thin soap film," Lab Chip **14**(18), 3525–3529 (2014).

[8]H. S. Hsieh and J. Lin, "Laser-induced vibration during pulsed laser forming," Opt. Laser Technol. **36**(6), 431–439 (2004).

[9]H. T. Huan, A. Mandelis, L. X. Liu, B. Lashkari, and A. Melnikov, "Application of linear frequency modulated laser ultrasonic radar in reflective thickness and defect non-destructive testing," NDT&E Int. **102**, 84–89 (2019).

[10]Y. X. Sun, D. N. Fang, M. Saka, and A. K. Soh, "Laser-induced vibrations of micro-beams under different boundary conditions," Int. J. Solids Struct. **45**(7), 1993–2013 (2008).

[11]N. M. Daud, M. K. Saidin, N. Bidin, and Y. M. Daud, *Laser Beam Modulation by an Acousto Optic Mode Locker. Faculty of Science* (University Teknologi, 2006), Vol. 1, pp. 16–21.

[12]M. Tarabini, B. Saggin, D. Scaccabarozzi, and G. Moschioni, "The potential of micro-electro-mechanical accelerometers in human vibration measurements," J. Sound Vib. **331**(2), 487–499 (2012).

[13]K. Medeiros, F. de Oliveira, C. Barbosa, and E. de Oliveira, "Optimization of flow rate measurement using piezoelectric accelerometers: Application in water industry," Measurement **91**, 576–581 (2016).

[14]J. Zhang, Y. Y. Cheng, Q. Xia, and Z. S. Wu, "Change localization of a steel-stringer bridge through long-gauge strain measurements," J. Bridge Eng. **21**(3), 04015057 (2016).

[15]G. Alfaro Degan, G. Coltrinari, and D. Lippiello, "Analysis of ground-transducer coupling in monitoring vibration from railways: A case study," Int. J. Transp. Dev. Integr. **1**(2), 300–310 (2017).

[16]M. Ueda, T. Yamaguchi, and H. Kakiuchi, "A simple optical method for measuring the vibration amplitude of a speaker," Opt. Lasers Eng. **32**(1), 21–28 (1999).

[17]B. Ferrer, J. Espinosa, J. Pérez, S. Ivorra, and D. Mas, "Optical scanning for structural vibration measurement," Res. Nondestruct. Eval. **22**(2), 61–75 (2011).

[18]D. Shetty, A. Ali, and J. Hill, "Optical instrumentation for vibration measurement and monitoring," Int. J. Precis. Eng. Manuf. **12**(3), 405–411 (2011).

[19]A. Chan, L. Mongeau, and K. Kost, "Vocal fold vibration measurements using laser Doppler vibrometry," J. Acoust. Soc. Am. **133**(3), 1667 (2013).

[20]H. H. Nassif, M. Gindy, and J. Davis, "Comparison of laser Doppler vibrometer with contact sensors for monitoring bridge deflection and vibration," NDT E Int. **38**(3), 213–218 (2005).

[21]A. B. Stanbridge, M. Martarelli, and D. J. Ewins, "Measuring area vibration mode shapes with a continuous-scan LDV," Measurement **35**(2), 181–189 (2004).

[22]Z. Li, A. Haigh, C. Soutis, and A. Gibson, "Principles and applications of microwave testing for woven and non-woven carbon fibre-reinforced polymer composites: A topical review," Appl. Compos. Mater. **25**(4), 965–982 (2018).

[23]*Principles of Near-Field Microwave Microscopy*, edited by S. M. Anlage, V. V. Talanov, and A. R. Schwartz (Springer NT, 2007).

[24]C. Gao and X. D. Xiang, "Quantitative microwave near-field microscopy of dielectric properties," Rev. Sci. Instrum. **69**(11), 3846–3851 (1998).

[25]G. Gramse, M. Kasper, L. Fumagalli, G. Gomila, P. Hinterdorfer, and F. Kienberger, "Calibrated complex impedance and permittivity measurements with scanning microwave microscopy," Nanotechnology **25**(14), 145703 (2014).

[26]G. Mansutti, A. T. Mobashsher, K. S. Bialkowski, B. J. Mohammed, and A. Abbosh, "Millimeter-wave substrate integrated waveguide probe for skin cancer detection," IEEE Trans. Biomed. Eng. **67**(9), 2462–2472 (2020).

[27]X. Jin, M. Farina, X. Wang, G. Fabi, X. Cheng, and J. C. M. Hwang, "Quantitative scanning microwave microscopy of the evolution of a live biological cell in a physiological buffer," IEEE Trans. Microw. Theory Tech. **67**(12), 5438–5445 (2019).

[28]A. G. Every, Z. N. Utegulov, and I. A. Veres, "Laser thermoelastic generation in metals above the melt threshold," J. Appl. Phys. **114**(20), 203508 (2013).

[29]*Measuring Copper Surface Roughness for High Speed Applications*, edited by J. A. Marshall (MacDermid Inc., 2015).

[30]F. Keilmann and R. Hillenbrand, "Near-field microscopy by elastic light scattering from a tip," Philos. Trans. R. Soc. A. **362**(1817), 787–805 (2004).

[31]B. A. Bagdad, C. Lozano, and F. Gamiz, "Near-field scanning microwave microscope platform based on a coaxial cavity resonator for the characterization of semiconductor structures," Solid-State Electron. **159**, 150–156 (2019).

[32]H. Guo, X. Li, Q. Zhu, Z. R. Zhang, Y. S. Liu, Z. H. Li, H. F. Wen, Y. J. Li, J. Tang, and J. Liu, "Imaging nano-defect of metal waveguides using the microwave cavity interference enhancement method," Nanotechnology **31**(45), 455203 (2020).

[33]S. S. Tuca, G. Badino, G. Gramse, E. Brinciotti, M. Kasper, Y. J. Oh, R. Zhu, C. Rankl, P. Hinterdorfer, and F. Kienberger, "Calibrated complex impedance of CHO cells and *E. coli* bacteria at GHz frequencies using scanning microwave microscopy," Nanotechnology **27**(13), 135702 (2016).

[34]M. F. Córdoba-Erazo, "Near-field microwave microscopy for surface and subsurface characterization of materials," Ph.D. dissertation (University of South Florida, 2015).

[35]*Field and Wave Electromagnetics*, edited by D. K. Cheng (Addison-Wesley, 1992).

[36]F. Duewer, C. Gao, and X. D. Xiang, "Tip-sample distance feedback control in a scanning evanescent microwave probe for nonlinear dielectric imaging," Rev. Sci. Instrum. **71**(6), 2414–2417 (2000).

[37]L. Wang, Z. X. Xia, Y. J. Cheng, and Y. Fan, "A frequency reconfigurable microwave reaction cavity based on a quarter-wave coaxial cavity resonator," in *International Symposium on Antennas, Propagation and EM Theory (ISAPE)* (IEEE, 2012), pp. 737–740.